J|A|C|S ARTICLES

Published on Web 09/09/2009

Tandem Mass Spectrometry of Thiolate-Protected Au Nanoparticles $Na_xAu_{25}(SC_2H_4Ph)_{18-y}(S(C_2H_4O)_5CH_3)_y$

Christina A. Fields-Zinna,[†] Jason S. Sampson,[‡] Matthew C. Crowe,[†,§] Joseph B. Tracy,[†,||] Joseph F. Parker,[†] Alexander M. deNey,[†,⊥] David C. Muddiman,[‡] and Royce W. Murray*[,†]

Kenan Laboratories of Chemistry, University of North Carolina, Chapel Hill, North Carolina 27599, and W. M. Keck FT-ICR Mass Spectrometry Laboratory, Department of Chemistry, North Carolina State University, Raleigh, North Carolina 27695

Received July 13, 2009; E-mail: rwm@email.unc.edu

Abstract: We report the first collision-induced dissociation tandem mass spectrometry (CID MS/MS) of a thiolate-protected Au nanoparticle that has a crystallographically determined structure. CID spectra assert that dissociation pathways for the mixed monolayer $Na_xAu_{25}(SC_2H_4Ph)_{18-y}(S(C_2H_4O)_5CH_3)_y$ centrally involve the semi-ring Au_2L_3 coordination (L = some combination of the two thiolate ligands) that constitutes the nanoparticle's protecting structure. The data additionally confirm charge state assignments in the mass spectra. Prominent among the fragments is $[Na_2AuL_2]^{1+}$, one precursor of which is identified as another nanoparticle fragment in the higher *m*/*z* region. Another detected fragment, $[Na_2Au_2L_3]^{1+}$, represents a mass loss equivalent to an entire semi-ring, whereas others suggest involvement (fragmentation/rearrangement) of multiple semi-rings, e.g., $[NaAu_3L_3]^{1+}$ and $[NaAu_4L_4]^{1+}$. The detailed dissociation/rearrangement mechanisms of these species are not established, but they are observed in other mass spectrometry experiments, including those under non-CID conditions, namely, electrospray ionization mass spectrometry (ESI-MS) with both time-of-flight (TOF) and FT-ICR analyzers. The latter, previously unreported results show that even soft ionization sources can result in Au nanoparticle fragmentation, including that yielding Au_4L_4 in ESI-TOF of a much larger thiolate-protected Au_{144} nanoparticle under non-CID conditions.

Introduction

The importance of our understanding of design and fabrication of nanoparticles has steadily increased as their potential applications have spread,[1−4] as for instance in biomedical[5−8] drug delivery transporters that rely on specific functionalities. Detailed chemical composition information for almost all such nanoparticle systems, such as gold nanoparticles protected by organothiolate ligand shells, is lacking; properties reported represent average data sets and lack molecular resolution. As materials prepared in the emerging science of nanotechnology become smaller and their uses more common, it becomes increasingly important to explicitly identify the composition and structure of these species, in order to understand and control their functioning.

Mass spectrometry is a powerful tool for accurate characterization of biologically relevant molecular species such as proteins and metabolites.[9−13] The use of mass spectrometry in nanotechnology studies has been mostly focused on mass determinations of various sizes and types of nanoparticles.[14−30] Such studies encounter the challenge of high mass and intrinsic

[†] University of North Carolina.
[‡] North Carolina State University.
[§] Current address: Dept. Chem., University of Washington, Seattle, Washington 98195.
[||] Current address: Dept. Mats. Sci. and Eng., North Carolina State University, Raleigh, NC 27695.
[⊥] Current address: Entegrion, PO Box 14867, Research Triangle Park, NC 27709.

(1) Eklund, S. E.; Cliffel, D. E. *Langmuir* **2004**, *20*, 6012–6018.
(2) Drechsler, U.; Erdogan, B.; Rotello, V. M. *Chem.−Euro. J.* **2004**, *10*, 5570–5579.
(3) Xiong, X.; Busnaina, A. *J. Nanopart. Res.* **2008**, *10*, 947–954.
(4) Fritzsche, W.; Csaki, A.; Moeller, R.; Steinbrueck, A.; Festag, G.; Wolff, A.; Schueler, T. *Proc. SPIE* **2008**, *6799*, 679906/679901–679906/679907.
(5) Liu, Y.; Miyoshi, H.; Nakamura, M. *Int. J. Cancer,* **2007**, *120*, 2527–2537.
(6) Oh, K. S.; Kim, R. S.; Lee, J.; Kim, D.; Cho, S. H.; Yuk, S. H. *J. Appl. Polymer Sci.* **2008**, *108*, 3239–3244.
(7) Singh, P.; Prasuhn, D.; Yeh, R. M.; Destito, G.; Rae, C. S.; Osborn, K.; Finn, M. G.; Manchester, M. *J. Controlled Release* **2007**, *120*, 41–50.
(8) Yaguee, C.; Moros, M.; Grazu, V.; Arruebo, M.; Santamaria, J. *Chem. Eng. J. (Amsterdam, Neth.)* **2008**, *137*, 45–53.
(9) Zhang, X.; Wei, D.; Yap, Y.; Li, L.; Guo, S.; Chen, F. *Mass Spectrom. Rev.* **2007**, *26*, 403–431.
(10) Domon, B.; Aebersold, R. *Science (Washington, DC, U. S.* **2006**, *312*, 212–217.
(11) Wei, X.; Li, L. *Int. J. Clin. Exp. Pathol* **2009**, *2*, 132–148.
(12) Papac, D. I.; Shahrokh, Z. *Pharm. Res.* **2001**, *18*, 131–145.
(13) Yeboah, F. K.; amdKonishi, Y. *Anal. Lett.* **2003**, *36*, 3271–3307.
(14) Whetten, R. L.; Khoury, J. T.; Alvarez, M. M.; Murthy, S.; Vezmar, I.; Wang, Z. L.; Stephens, P. W.; Cleveland, C. L.; Luedtke, W. D.; Landman, U. *Adv. Mater.* **1996**, *8*, 428–433.
(15) Jimenez, V. L.; Georganopoulou, D. G.; White, R. J.; Harper, A. S.; Mills, A. J.; Lee, D.; Murray, R. W. *Langmuir* **2004**, *20*, 6864–6870.
(16) McNeal, C. J.; Hughes, J. M.; Pignolet, L. H.; Nelson, L. T. J.; Gardner, T. G.; Fackler, J. P., Jr.; Winpenny, R. E. P.; Irgens, L. H.; Vigh, G.; Macfarlane, R. D. *Inorg. Chem.* **1993**, *32*, 5582–5590.
(17) Negishi, Y.; Chaki, N. K.; Shichibu, Y.; Whetten, R. L.; Tsukuda, T. *J. Am. Chem. Soc.* **2007**, *129*, 11322–11323.
(18) Chaki, N. K.; Negishi, Y.; Tsunoyama, H.; Shichibu, Y.; Tsukuda, T. *J. Am. Chem. Soc.* **2008**, *130*, 8608–8610.

10.1021/ja905787y CCC: $40.75

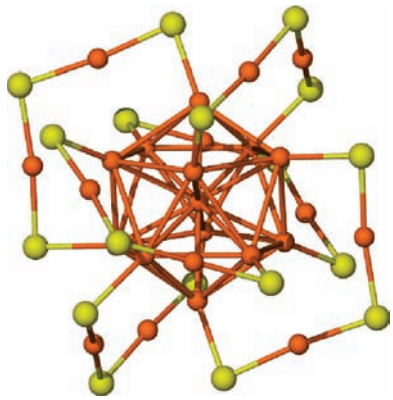

Figure 1. Crystal structure of $Au_{25}(SCH_2CH_2Ph)_{18}$, where smaller orange balls are Au atoms, and larger yellow balls are sulfur atoms (the rest of the ligand, $-CH_2CH_2Ph$, is not pictured). Image emphasizes the Au_2L_3 semi-rings that are found in this paper to comprise central fragmentation/rearrangement patterns in CID experiments.

nonvolatility of metal salt clusters and metal nanoparticles. Laser desorption ionization (LDI)[14,15] and plasma desorption (PD)[16] have been effectively used but produce mass spectra showing extensive fragmentation, complicating interpretation. Alternative techniques have been explored seeking minimal fragmentation, utilizing "soft" ionization sources such as electrospray ionization (ESI)[17−21,25] and matrix-assisted laser desorption ionization (MALDI).[22] Although not devoid of fragmentation, these explorations have established ESI and MALDI as viable methods for obtaining mass spectra of very small nanoparticles.

The exact molecular formula of the nanoparticle $[Au_{25}(SC_2H_4Ph)_{18}]^{1-}$ has been defined by mass spectrometry, and importantly, the actual structural arrangement has been established by a subsequent crystal structure determination of its native[31] (−1) and oxidized forms.[32] Interest is now propelled toward understanding the chemistry of its "semi-ring" coordination shell (which we assume here is not altered by exchanges of thiolate ligands). The detailed structure[31] is shown in Figure 1; the organothiolate ligands are all in bridging coordination in six core-protecting Au_2L_3 semi-rings bonded to a Au_{13} core. This structure is buttressed by supporting density functional theory calculations,[33] and earlier crystallography[34] of a $Au_{102}L_{44}$ nanoparticle that shows analogous, but shorter, semi-rings.

Even "soft" ESI[23−25,27,29,30] and MALDI[22,23] ionization sources produce mass spectra containing lower mass fragments of metal and metal sulfide nanoparticles. The pathways for such fragmentation are generally poorly understood and for Au nanoparticles, unstudied. Detection of fragments associated with a precursor of known initial structure, such as the $Au_{25}(SC_2H_4Ph)_{18}$ nanoparticle, would provide reactivity data to confirm the possible origin of the fragments and as illustrated for semiconductor nanoparticles by Strouse et al.[24,25] ultimately allow detection of fragments from other nanoparticles to shed light on their parent structures. Organic MS now routinely uses tandem mass spectrometry to determine ion charges and bonding patterns (i.e., sequencing) from known cleavage propensities established by extensive prior investigations. *No information of the latter sort exists for thiolate-protected Au nanoparticles, as only recently have structures been determined.*[31,32,34]

With this in mind, we have investigated and present here low-energy collision-induced dissociation tandem mass spectrometry (CID MS/MS) data for mixed monolayer $Au_{25}L_{18}$ nanoparticles. L represents a mixture of $-SC_2H_4Ph$ and monodisperse methoxy penta(ethyleneglycol) thiolate ligands ($-SC_2H_4Ph$ is abbreviated as -SC2Ph and the $-S(CH_2CH_2O)_5CH_3$ ligand as -SPEG.) The -SPEG ligands are introduced by ligand exchanges with the original -SC2Ph ligands. The fragment formula assignments from CID MS/MS experiments are confirmed using ESI-TOF-MS and high resolution ESI-FTICR-MS data. The resulting fragment spectra reveal dissociation products of the nanoparticle semi-rings and additionally, by observing fragments such as $Au_4L_4^{1+}$, assert the occurrence of semi-ring rearrangements on the surface of the nanoparticle. In addition, experiments *not* under CID conditions yield similar fragmentation from the $Au_{25}L_{18}$ nanoparticle. Similar fragments are also found in non-CID spectra of a much larger Au_{144} nanoparticle, implying surface structural features that are similar to those of $Au_{25}L_{18}$ nanoparticles.

The purpose of incorporation of the -SPEG ligand into the nanoparticle ligand shell ("PEGylation" of the nanoparticle) is to facilitate its cationization[20] in electrospray experiments. PEG is a known electrospray tag and readily coordinates to protons and/or alkali metal ions.[35] Addition of sodium acetate, by multiple Na^+/-SPEG associations, also lowers the nanoparticle *m/z* values (below 4000 *m/z*), easing both detection and the task of mass calibration, as previously reported.[20,36] Intrinsically, as a result of the statistics of ligand exchanges,[20,21,26] the mixed monolayer $Na_xAu_{25}(SC_2H_4Ph)_{18-y}(S(C_2H_4O)_5CH_3)_y$ nanoparticles have a distribution of numbers of the two different ligands, i.e., *y* is variable, but the total ligand count remains at 18. Mass spectra of such mixed monolayer Au nanoparticles display this ligand count distribution by showing peaks spaced by 130 Da (the mass difference between the two ligands). This peak spacing is *also* seen in detected low-mass fragment species in CID

(19) Bertino, M. F.; Sun, Z.-M.; Zhang, R. and; Wang, L.-S. *J. Phys. Chem. B* **2006**, *110*, 21416–21418.
(20) Tracy, J. B.; Kalyuzhny, G.; Crowe, M. C.; Balasubramanian, R.; Choi, J.-P.; Murray, R. W. *J. Am. Chem. Soc.* **2007**, *129*, 6706–6707.
(21) Tracy, J. B.; Crowe, M. C.; Parker, J. F.; Hampe, O.; Fields-Zinna, C. A.; Dass, A.; Murray, R. W. *J. Am. Chem. Soc.* **2007**, *129*, 16209–16215.
(22) Dass, A.; Stevenson, A.; Dubay, G. R.; Tracy, J. B.; Murray, R. W. *J. Am. Chem. Soc.* **2008**, *130*, 5940–5946.
(23) Schaaff, T. G.; Whetten, R. L. *J. Phys. Chem. B* **2000**, *104*, 2630–2641.
(24) Gaumet, J. J.; Strouse, G. F. *J. Am. Soc. Mass Spectrom.* **2000**, *11*, 338–344.
(25) Gaumet, J. J.; Khitrov, G. A.; Strouse, G. F. *Nano Lett.* **2002**, *2*, 375–379.
(26) Dass, A.; Holt, K.; Parker, J. F.; Feldberg, S. W.; Murray, R. W. *J. Phys. Chem. C* **2008**, *112*, 20276–20283.
(27) Cliffel, D. E.; Zamborini, F. P.; Gross, S. M.; Murray, R. W. *Langmuir* **2000**, *16*, 9699–9702.
(28) Dass, A.; Dubay, G. R.; Fields-Zinna, C. A.; Murray, R. W. *Anal. Chem.* **2008**, *80*, 6845–6849.
(29) Lover, T.; Henderson, W.; Bowmaker, G. A.; Seakins, J. M.; Cooney, R. P. *Inorg. Chem.* **1997**, *36*, 3711–3723.
(30) Lover, T.; Henderson, W.; Bowmaker, G. A.; Seakins, J. M.; Cooney, R. P. *Chem. Mater.* **1997**, *9*, 1878–1886.
(31) Heaven, M. W.; Dass, A.; White, P. S.; Holt, K. M.; Murray, R. W. *J. Am. Chem. Soc.* **2008**, *130*, 3754–3755.
(32) Zhu, M.; Aikens, C. M.; Hollander, F. J.; Schatz, G. C.; Jin, R. *J. Am. Chem. Soc.* **2008**, *130*, 5883–5885.
(33) Akola, J.; Walter, M.; Whetten, R. L.; Hakkinen, H.; Gronbeck, H. *J. Am. Chem. Soc.* **2008**, *130*, 3756–3757.
(34) Jadzinsky, P. D.; Calero, G.; Ackerson, C. J.; Bushnell, D. A.; Kornberg, R. D. *Science* **2007**, *318*, 430–433.
(35) Wong, S. F.; Meng, C. K.; Fenn, J. B. *J. Phys. Chem.* **1988**, *92*, 546–550.
(36) Fields-Zinna, C. A.; Crowe, M. C.; Dass, A.; Weaver, J. E. F.; Murray, R. W. *Langmuir* **2009**, *25*, 7704–7710.

spectra, there again reflecting various fragmentations of the core-protecting nanoparticle [Au_2L_3] semi-rings.

Experimental Methods

Chemicals. Phenylethylenethiol ($HSCH_2CH_2Ph$, or HSC2Ph, 98%), hexanethiolate (HSC_6H_{13}, 95%), tetrabutylammonium perchlorate (Bu_4NClO_4, >99%), tetra-*n*-octylammonium bromide (Oct_4NBr, 98%), sodium borohydride ($NaBH_4$, 99%), sodium acetate (NaOAc, > 99.0%), and cesium acetate (CsOAc, 99.9%) were obtained from Sigma-Aldrich. Certified ACS toluene, optima methylene chloride, optima methanol, optima acetonitrile, and absolute ethanol (Fischer) were used as received. Water was purified with a Barnstead NANOpure system (18 MΩ). Hydrogen tetrachloroaurate trihydrate (from 99.999% pure gold) was prepared by a literature procedure[37] and stored in a freezer at −20 °C. The PEGylated thiol (methoxy penta(ethyleneglycol) thiol, HS-$(CH_2CH_2O)_5CH_3$ or HSPEG) was prepared according to a literature method,[38] and the mass spectrum of our synthetic product is presented in a previous publication.[36] The ammonium thiol exchanged onto $Au_{144}(SC_6H_{13})_{59}$ was *N*,*N*,*N*-trimethyl(11-mercaptoundecyl)-ammonium hexafluorophosphate ($[HSC_{11}H_{22}N^+(CH_2CH_3)_3][PF_6^-]$, (HS-TMA), $[HS\text{-}TMA^+][PF_6^-]$), and was synthesized as previously described.[27,39] Briefly, trimethylamine in methanol solution was added to 11-bromo-1-undecene in methanol at a 3:1 molar ratio and stirred for 2 days at room temperature, resulting in 1-undecene terminated with a quaternary ammonium bromide. The solution was dried with a rotary evaporator, resulting in a viscous yellow liquid, which was precipitated several times with large volumes of hexanes and then dissolved in dichloromethane. Thioacetic acid was added to the solution in a 3:1 molar ratio and stirred at room temperature while irradiated with an SP-200 mercury light source, resulting in the thioester terminated alkylammonium salt. The reaction mixture was dried, and the product washed several times with diethyl ether. To convert the thioester into the thiol, the alkylammonium salt was dissolved in 10% HCl and refluxed at 90−100 °C for 1 h. The water was removed in vacuo, resulting in a solid white product $[HSC_{11}H_{22}N^+(CH_2CH_3)_3][Cl^-]$, or $[HS\text{-}TMA^+][Cl^-]$). The chloride anion was exchanged with hexafluorophosphate ($[HS\text{-}TMA^+][Cl^-]$), by dissolving the product in methanol with three times the molar equivalent of potassium hexafluorophosphate and stirring for 24 h. After evaporation of the methanol, the product was dissolved in dichloromethane, leaving excess potassium salts behind. The resulting solution was vacuum filtered, and the collected sample was dried. This process was repeated to ensure complete replacement of the chloride ions, ($[HS\text{-}TMA^+][PF_6^-]$), as confirmed with 1H NMR in D_2O (data not shown) as previously described.[39]

Synthesis of Nanoparticles: $[Oct_4N^+][Au_{25}(SCH_2CH_2Ph)_{18}^-]$. $[Oct_4N^+][Au_{25}(SCH_2CH_2Ph)_{18}^-]$ (or just $Au_{25}(SC2Ph)_{18}$) nanoparticles were synthesized as previously reported,[40] though wrongly assigned in that paper as being $Au_{38}(SCH_2CH_2Ph)_{24}$. $AuCl_4^-$ (as 1.9 g of $HAuCl_4$) was transferred from an aqueous phase to a 45 mM Oct_4NBr in toluene (126 mL), and after adding 2.17 mL of phenylethanethiol (HSC2Ph), stirred in toluene overnight. In this reaction, the mole ratio of thiol to metal was 3.2:1. The colorless solution of mixed metal thiolates was cooled to 0 °C in an ice water bath, 2.4 g of $NaBH_4$ in 38 mL ice cold Nanopure water was added, and the solution stirred vigorously for 24 h. Discarding the aqueous layer, the organic layer was washed three times with Nanopure water and rotary evaporated to a viscous sludge. The sludge was extracted with ethanol for about 2 h to remove excess ligand and larger nanoparticles. The ethanol-insoluble portion, containing the small-sized nanoparticles, was further filtered and purified using repeated solvent fractionation, using acetonitrile to dissolve the nanoparticle sample, precipitating nanoparticles by methanol addition, removing excess ligand, and gradually purifying the small nanoparticle content. The acetonitrile/methanol treatments were performed several more times for purification and isolation of small nanoparticles.

Synthesis of Nanoparticles: $Au_{144}(SC_6H_{13})_{59}$. The synthesis of this 1.6 nm nanoparticle, previously termed "Au_{140}", has been described[41] but will be reviewed here. A 3.1 g portion of $HAuCl_4$ was added to water and transferred from aqueous phase to a 45 mM Oct_4NBr in toluene. Next, 3.33 mL of hexanethiol (HSC_6H_{13}), or a 3:1 thiol/metal mole ratio, was added to the solution, which was stirred until clear. The solution was cooled to 0 °C, 3.8 g of $NaBH_4$ in 20 mL of ice-cold Nanopure water was added, and the solution was stirred vigorously for 1 h. Discarding the aqueous layer, the organic layer was washed three times with Nanopure water and was rotary evaporated to a viscous sludge. The ethanol-soluble portion was collected overnight, filtered to remove larger nanoparticles, dried, and treated with acetonitrile to remove smaller nanoparticles, excess ligands, and salts.

Ligand Exchanges. A previously reported[20] procedure was used for exchanging phenylethanethiolate ligands (-SC2Ph) of $Au_{25}(SCH_2CH_2Ph)_{18}$ with methoxy penta(ethyleneglycol) thiolate ligands (-SPEG = $-S(CH_2CH_2O)_5CH_3$) (mass = 268.13 Da). Briefly, 2 μL (0.72 mmol) of the PEGylated thiol was added to about 1 mg (0.14 μmol) of nanoparticle sample dissolved in about 200 μL methylene chloride (an excess of 62 ligands per nanoparticle). This was stirred for 24 h and dried on a rotary evaporator, and excess ligand was removed by washing several times with heptane.

For exchanging $-SC_{11}H_{22}N(CH_2CH_3)_3^+$, or (-S-TMA$^+$), onto $Au_{144}(SC_6H_{13})_{59}$ (or Au_{144}), 0.02 μmol of *N*,*N*,*N*-trimethyl(11-mercaptoundecyl)ammonium hexafluorophosphate ($[HS\text{-}TMA^+][PF_6^-]$) was added to 0.14 μmol of Au_{144} in 300 μL of methylene chloride for 48 h. The sample was dried and washed of excess ligands with acetonitrile.

ESI-QQQ-MS/MS. Positive-mode CID spectra were obtained on a Micromass Quattro II, a triple quad mass spectrometer with a nanoelectrospray ionization source. For PEGylated (mixed -SC2Ph and -SPEG ligand shell) $Au_{25}L_{18}$, the 69 μM nanoparticle solutions in optima MeOH (for solubility plus ESI compatibility) contained sodium acetate (NaOAc) at a mole ratio of 75:1 sodium/nanoparticle, aiming at coordination of Na^+ to the PEG chains. Instrumental parameters were set for optimal detection of the molecular ions, precursor ions, and fragment ions, with the capillary set at 1.33 V and cone set at 25 V. Collision voltages used were between 75−100 V; changes in voltages resulted simply in intensity changes in signal and not changes in the presence of species. The collision gas used was argon. The data were smoothed using the Savitsky−Golay (17-point quadratic) method.[42] For high resolution assignments of molecular formulas, the publicly available software Molecular Weight Calculator was used to produce simulated mass spectra for comparison to experiment.

ESI-TOF-MS. Positive-mode ESI-MS spectra were acquired on a Bruker BioTOF II instrument (Billerica, MA), a reflectron time-of-flight mass spectrometer equipped with an Apollo electrospray ionization source. The 50 μM PEGylated Au_{25} nanoparticle solutions in 75% optima methanol/25% dichloromethane (for solubility plus ESI compatibility) contained sodium acetate (NaOAc) at a mole ratio of 75:1 sodium/nanoparticle, for cationizing the nanoparticle through the coordination of Na^+ to the PEG chain. The 25 μM ammonium-thiolated Au_{144} nanoparticle solution was run in 70:30 chloroform/methanol. The ESI source was operated with flow rates of 60−90 μL/h, the ion transfer time was set at 120 μs, and 50,000 scans were averaged in the data presented. Calibration was determined externally by observing clusters ($Cs(CsOAc)_n^+$) of

(37) Brauer, G. *Handbook of Preparative Inorganic Chemistry*; Academic Press: New York, 1965.
(38) Snow, A. W.; Foos, E. E. *Synthesis* **2003**, 509–512.
(39) Tien, J.; Terfort, A.; Whitesides, G. *Langmuir* **1997**, *13*, 5349–5355.
(40) Donkers, R. L.; Lee, D.; Murray, R. W. *Langmuir* **2004**, *20*, 1945–1952.
(41) Hicks, J. F.; Templeton, A. C.; Chen, S.; Sheran, K. M.; Jasti, R.; Murray, R. W.; Debord, J.; Schaaff, T. G.; Whetten, R. L. *Anal. Chem.* **1999**, *71*, 3703–3711.
(42) Savitzky, A.; Golay, M. J. E. *Anal. Chem.* **1964**, *36*, 1627–1639.

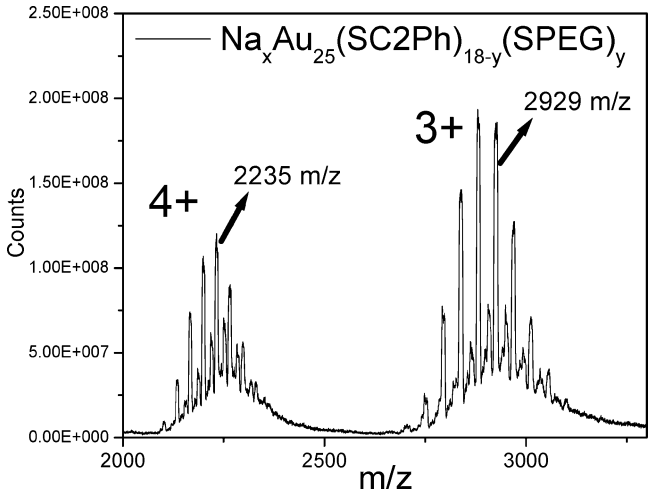

Figure 2. ESI-QQQ-MS spectrum of $Au_{25}(SC2Ph)_{18}$ after PEGylation via ligand exchange with HSPEG thiol (3:1 thiol/MPC). Nanoparticle solutions in MeOH contained 75:1 NaOAc/nanoparticle. The multiple large 3+ and 4+ peaks represent different values of y and are due to the statistics of the ligand exchanges.[20,21,26] Peaks at 2235 *m/z* and 2929 *m/z* are selected as molecular ions for fragmentation; they represent the species $[Na_5Au_{25}(SC2Ph)_7(SPEG)_{11}]^{4+}$ and $[Na_4Au_{25}(SC2Ph)_8(SPEG)_{10}]^{3+}$, respectively.

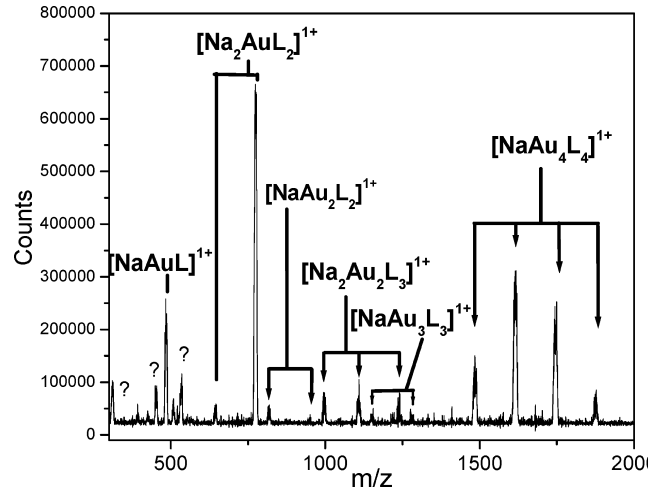

Figure 3. ESI-QQQ-MS/MS spectrum of PEGylated Au_{25} sample (in methanol with excess NaOAc) after fragmentation under CID conditions. The CID spectrum shows low *m/z* fragment ions produced from $[Na_4Au_{25}(SC2Ph)_8(SPEG)_{10}]^{3+}$ (*m/z* = 2929). (The low *m/z* CID spectrum of $[Na_4Au_{25}(SC2Ph)_7(SPEG)_{11}]^{4+}$ (*m/z* = 2235) is quite similar, with the exception of not showing fragments $[NaAuL]^{1+}$ and $[NaAu_3L_3]^{1+}$). Brackets and arrows indicate Au_NL_M species, where L is a distribution of ligands (SC2Ph and SPEG) in which SPEG is more prominent. The AuL_2 and Au_4L_4 species have the highest intensity peaks.

cesium acetate, as well as internally, using $Au_{25}L_{18}$ as a standard since its structure and mass are known. The data were processed as described above.

ESI-FTICR-MS. Positive-mode nanoESI spectra of a 50 μM PEGylated Au_{25} sample in optima methanol (containing sodium acetate (NaOAc) at a mole ratio of 50:1 sodium/nanoparticle) were obtained by direct infusion through a 75 μm i.d. fused silica capillary (Polymicro Technologies, Phoenix, AZ) connected using a stainless steel union (VICI, Houston, TX) to a 30 μm tapered fused silica Picotip (New Objective Inc., Woburn, MA) at a flow rate of 1.5−2.8 μL/min. High voltage (2.6−2.8 kV) was applied at the union to produce stable electrospray which was detected using a hybrid LTQ-FT-ICR mass spectrometer (Thermo Electron Inc., San Jose, CA). The LTQ-FT-ICR was equipped with a 7 T actively shielded superconducting magnet, and the resolving power was set to 100,000 at 400 *m/z*. The maximum ionization time was set to 2000 ms for MS data and 8000 ms for MS/MS.

Results and Discussion

The exact mass of the $Au_{25}(SC2Ph)_{18}$ nanoparticle is known from its detailed crystal structure[31] (Figure 1) and from previous mass spectrometry using various ionization approaches.[20−22] As discussed in the Introduction, PEGylation of the $Au_{25}(SC2Ph)_{18}$ nanoparticle was accomplished by ligand exchange with the monodisperse (methoxy penta(ethyleneglycol) thiol (-SPEG); we have found this mode[20] of nanoparticle cationization very reliable for this small nanoparticle. Figure 2 shows the mass spectra of 3+ and 4+ mixed monolayer nanoparticles, having composition $[Na_4Au_{25}L_{18}]^{3+}$ and $[Na_5Au_{25}L_{18}]^{4+}$ where L, the -SC2Ph and -SPEG ligands, always sums to a total of 18. Both distributions of peaks show a spacing of 130 Da, which is the difference in the -SC2Ph and -SPEG ligand masses; the different peaks reflect the different relative numbers of the two ligands on individual nanoparticles. Figure S-1 (see Supporting Information) provides an example of a high resolution ESI-FT-ICR spectrum of the 3+ nanoparticle mixed monolayer distribution and a close-up spectrum of the particular PEGylated ion $[Na_4Au_{25}(SC2Ph)_8(SPEG)_{10}]^{3+}$ showing isotopic resolution that confirms its 3+ charge state assignment.

The precursor ions for the low-energy CID fragmentation MS/MS experiments were members of the peak distributions shown in Figure 2, namely, the intense peaks $[Na_4Au_{25}(SC2Ph)_8(SPEG)_{10}]^{3+}$ and $[Na_5Au_{25}(SC2Ph)_7(SPEG)_{11}]^{4+}$, where *m/z* = 2929 and 2235, respectively. The charge on these ions is a combination of the number of Na^+ ions associated with the nanoparticle and the 1− charge of the native nanoparticle core.[20] The high resolution spectrum of Figure S-1 in Supporting Infomration is of the former of these two ions. Despite the small difference in the mixed monolayer compositions, the fragmentation of these two precursors, using 70−150 eV collision voltages, yielded nearly identical fragment spectra in the 0−2000 *m/z* region.

Figure 3 shows the fragment spectrum of the low *m/z* region for precursor ion *m/z* = 2929; we can identify the fragments $[NaAuL]^{1+}$, $[Na_2AuL_2]^{1+}$, $[NaAu_2L_2]^{1+}$, $[Na_2Au_2L_3]^{1+}$, $[NaAu_3L_3]^{1+}$, and $[NaAu_4L_4]^{1+}$. (The low mass spectrum for precursor ion *m/z* = 2235 (see Supporting Information, Figure S-2) includes all of these fragments except $[NaAuL]^{1+}$ and $[NaAu_3L_3]^{1+}$.) The fragment peaks corresponding to the same Au/L composition, L being some combination of -SC2Ph and -SPEG, are indicated by pointing brackets. For example, the four right-most bracketed peaks at *m/z* = 1490, 1620, 1750, and 1880 (collectively labeled $[NaAu_4L_4]^{1+}$) correspond to $[NaAu_4(SC2Ph)_a(SPEG)_b]^{1+}$ where *a/b* = 3/1, 2/2, 1/3, and 0/4, respectively. Note that no peak appears at 1360 for *a/b* = 4/0. Na^+ cationization is favored by the presence of the -SPEG ligand in the fragment; Na^+ is less efficiently associated[21] with solely -SC2Ph ligands. This difference in cationization of the fragment according to the ligands present is also seen for the peaks at 648 and 778 (labeled $[Na_2AuL_2]^{1+}$) for $[Na_2Au(SC2Ph)_a(SPEG)_b]^{1+}$ where *a/b* = 1/1 and 0/2, but not 2/0. The peak for *a/b* = 1/1 is by far the smaller of the two; this unfavored fragment contains two Na^+ ions but only one -SPEG ligand and one -SC2Ph ligand. The efficiency of cationization and detection of the fragment according to its -SPEG ligand content complicates discerning the relative efficiencies with which particular kinds of fragments are actually produced by the low-energy CID process but does not prevent some interferences from being drawn, as shown below.

The most prominent CID product in Figure 3 is the $[Na_2AuL_2]^{1+}$ fragment containing two -SPEG ligands (m/z = 778 Da). That the -SPEG ligand cationization influence is not a completely dominant effect on the observed fragment intensities can be seen by comparing the intensity of the $m/z = 778$ ion with that of other fragment ions containing two -SPEG ligands; note the smaller peaks for $[Na_2Au_2L_3]^{1+}$ at $m/z = 1100$ and $[NaAu_4L_4]^{1+}$ at $m/z = 1620$. The $[Na_2AuL_2]^{1+}$ fragment must represent a favored dissociation pathway, which considering the Au_2L_3 semi-rings (Figure 1) can be envisioned to occur by cleavage of two Au−S bonds within a single semi-ring. The Au−S bond has a polar-covalent character.[42] In Figure S-3 in Supporting Information, this peak in the experimental spectrum is matched with a corresponding calculated simulation.

Another fragment in Figure 3, $[Na_2Au_2L_3]^{1+}$, is equivalent to the loss of an entire semi-ring. The composition and charge (considering the two Na^+) of this fragment are consistent with previous theoretical analysis[33] of the semi-ring as a protecting $[Au_2L_3]^{1-}$ "ligand". Even though two of the $[Na_2Au_2L_3]^{1+}$ fragment peaks have -SPEG content equal to and greater than the above-discussed $[Na_2AuL_2]^{1+}$, they are *collectively* not as prominent in peak intensity. It seems that loss of a complete semi-ring, $[Au_2L_3]^{1-}$, which could occur by cleavage of two Au(core)-S bonds, is less favored than the cleavages that produce $[Na_2AuL_2]^{1+}$.

Another aspect of the fragments seen in Figure 3 is the charge of the Au-ligand complex. In all of the $[NaAu_NL_N]^{1+}$ fragments (e.g., $[NaAuL]^{1+}$, $[NaAu_2L_2]^{1+}$, $[NaAu_3L_3]^{1+}$, and $[NaAu_4L_4]^{1+}$), the Au-ligand complex is formally neutral. MS spectra obtained of synthesized cyclic gold(I)-thiolate tetramers (Au_4L_4) agree with this assignment.[43] In the $[Na_2Au_NL_{N+1}]^{1+}$ fragments (e.g., $[Na_2AuL_2]^{1+}$ and $[Na_2Au_2L_3]^{1+}$), however, the Au-ligand complexes all have a 1^- charge. Theory[44] predicts ring-like structures for Au_NL_N species, where the Au−S bonds exhibit a covalent bond character. The additional ligand in the Au_NL_{N+1} complexes is effectively added as a thiolate anion and may introduce some structural distortion relative to Au_NL_N. There is, however, no general difference in the intensities of the two kinds of complexes ($[NaAu_NL_N]^{1+}$ and $[NaAu_NL_N]^{1+}$).

Another prominent nanoparticle fragment seen in Figure 3 (right-hand bracket) is $[NaAu_4L_4]^{1+}$. The Au_4L_4 species has been encountered in other (non-CID) experiments[22,23,43,45] and calculations.[46] Both Au_4L_4 and AuL_2 were detected as electrospray dissociation products of a nanoparticle[23] (reported as Au_{28}(glutathione)$_{16}$ but now reassigned[37] as a Au_{25} nanoparticle), and in electrospray experiments on solutions preceding nanoparticle formation[43] and on a pharmaceutical product containing thiomalato-*S*-aurate(I).[45] Theory predicts[44] Au_4L_4 is a cyclical entity that is particularly stable in comparison to other cyclical Au_NL_N complexes. Considering the structure of the $Au_{25}L_{18}$ nanoparticle, and its Au_2L_3 semi-rings (Figure 1), the $[NaAu_4L_4]^{1+}$ peaks seen in Figure 3 clearly signal the presence of a multistep rearrangement of ligands involving at least two semi-rings on the Au_{13} core surface, presumably prior to fragment dissociation. A loss of $[NaAu_4L_4]^{1+}$ should yield $[Au_{21}L_{14}]^{1-}$, where the 13 Au atom core of $Au_{25}L_{18}$ would still be intact. The $[Au_{21}L_{14}]^{1-}$ fragment is not seen in this work, as seen further in this paper, but it has been seen with MALDI.[22] In another example, theoretical structures of Au_{21}[47] also show the 13 Au atom core still intact. Among the diverse structures that have been suggested for small nanoparticles,[33,48,49] semi-ring rearrangements would certainly seem to be conceivable. The literature offers other examples of novel and unexpected rearrangements of traditional molecules, for example, amino acids.[50]

As previously mentioned, for fragments like $[Na_2AuL_2]^{1+}$, the predominance of the $[Na_2Au(SPEG)_2]^{1+}$ peak as compared to $[Na_2Au(SC2Ph)(SPEG)]^{1+}$ would seem to be decided by cationization efficiency. On the other hand, within the Au_4L_4 set of peaks, the peak intensities appear to have no bias toward a ligand composition dominated by -SPEG; indeed, $Au_4(SPEG)_4$ has the lowest intensity of this set. Rather, the relative intensities of the Au_4L_4 peaks seem to resemble the coefficients of a binomial expansion distribution.[26] This points to the role of the random nature of ligand exchange; the relative locations of -SC2Ph and -SPEG ligands on the semi-rings are random. As a consequence, the compositions of semi-ring fragments produced during CID conditions reflect the randomness of ligand locations on the precursor ion. This statistical factor must thus be balanced against the reliance on a fragment's cationization efficiency, as ultimately the presence of a fragment ion is dependent on a cationizing agent (in this case, -SPEG).

Here we should mention a related, MALDESI experiment. A 50 μm solution of PEGylated $Au_{25}L_{18}$ containing NH_4OAc (75:1 NH_4OAc/MPC) was analyzed with a hybrid atmospheric pressure ionization source matrix-assisted laser desorption electrospray ionization (MALDESI)[51] coupled to FT-ICR mass spectrometry; no matrix was used. The stainless steel sample target was biased at 475 V while electrospraying 70:30 methanol/dichloromethane for ESI postionization of the laser desorbed neutral nanoparticles. The spectrum (data not shown) parallels the 3+ and 4+ charge state peaks seen in Figure 2 except with NH_4^+ ions coordinated rather than Na^+ ions. The experiments further validate the preceding mass and charge assignments.

Most of the small nanoparticle fragment ions seen in Figure 3 also appear in electrospray spectra in which no CID was performed. In both ESI-TOF-MS (Figure S-4, Supporting Information) and ESI-FTICR-MS (Figure 4), low mass fragment ions are seen that are identical to those found with ESI-QQQ-MS/MS (Figure 3), including AuL_2, Au_2L_3, Au_3L_3 and Au_4L_4 with various ligand compositions as seen in Figure 3. Figure 4 shows the low m/z range of a ESI-FTICR-MS spectrum of an intact, PEGylated $Au_{25}L_{18}$ nanoparticle (as shown in Figure 2) The Figure 4 spectrum is a $[NaAu_4L_4]^{1+}$ fragment, seen at isotopic resolution and further confirming the assignments of the analogous CID-produced fragment in Figure 3. A slightly lower resolution spectrum of this species obtained using ESI-TOF is shown in Figure S-4 (see Supporting Information). The presence of fragments such as seen in Figures 4 and S-4, under

(43) Gies, A. P.; Hercules, D. M.; Gerdon, A. E.; Cliffel, D. E. *J. Am. Chem. Soc.* **2007**, *129*, 1095–1104.
(44) Gronbeck, H.; Walter, M.; Hakkinen, H. *J. Am. Chem. Soc.* **2006**, *128*, 10268–10275.
(45) Howard-Lock, H. E.; LeBlanc, D. J.; Lock, C. J. L.; Smith, R. W.; Wang, Z. *Chem. Commun. (Cambridge)* **1996**, 1391–1392.
(46) Hakkinen, H.; Walter, M.; Gronbeck, H. *J. Phys. Chem. B* **2006**, *110*, 9927–9931.
(47) Femoni, C.; Iapalucci, M. C.; Longoni, G.; Tiozzo, C.; Zacchini, S. *Angew. Chem., Int. Ed.* **2008**, *47*, 6666–6669.
(48) Hakkinen, H.; Walter, M.; Groenbeck, H. *J. Phys. Chem. B* **2006**, *110*, 9927–9931.
(49) Iwasa, T.; Nobusada, K. *J. Phys. Chem. C* **2007**, *111*, 45–49.
(50) Vachet, R. W.; Bishop, B. M.; Erickson, B. W.; Glish, G. L. *J. Am. Chem. Soc.* **1997**, *119*, 5481–5488.
(51) Sampson, J. S.; Hawkridge, A. M.; Muddiman, D. C. *J. Am. Soc. Mass Spectrom.* **2006**, *17*, 1712–1716.

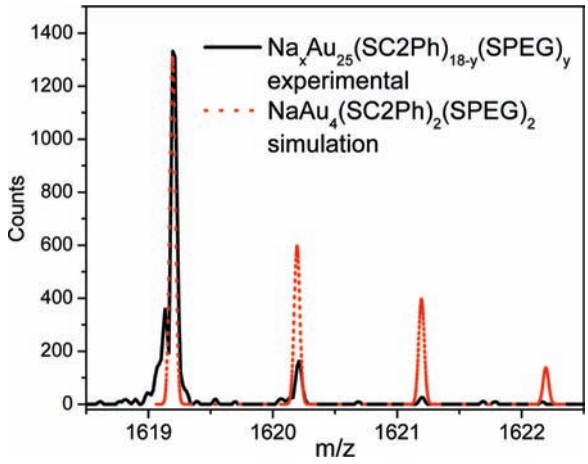

Figure 4. ESI-FTICR spectrum of $NaAu_4L_4$ fragments from the PEGylated $Au_{25}L_{18}$ sample in methanol, acquired *without* CID conditions. Experimental data is shown with a solid black line, and the simulation curve by a dotted red line. This isotopic resolution under non-CID conditions confirms assignments from lower resolution ESI-QQQ-MS/MS experiment, as well as revealing that $Au_{25}L_{18}$ fragments during the ESI spraying process.

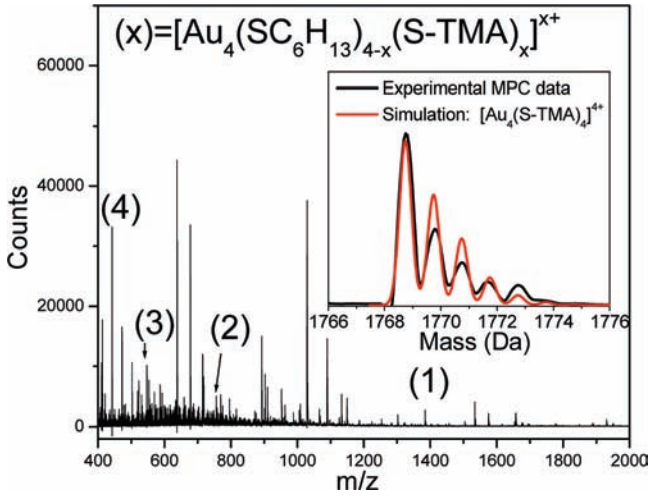

Figure 5. ESI-TOF-MS data of a "Au_{144}" sample with a hexanethiolate monolayer that has undergone ligand exchange with $[HSC_{11}N^+(CH_3)_3][Cl^-]$ or HS-TMA. Among the many low mass peaks in the spectrum can be found Au_4L_4 fragments of the parent ion that are ionized via the presence of the ammonium ligands. The Au_4L_4 peaks are labeled with (number), e.g., the number of -S-TMA ligands (which directly determines *z*) that are bound to the cyclic gold tetramer. The inset shows a close-up of one experimental (black) peak, $[Au_4(S\text{-}TMA)_4]^{4+}$, and a simulation (red). No other familiar fragments were identified.

non-CID electrospray conditions, with a "soft" ionization source, might have been previously explained by suggesting that they were contaminants of the nanoparticle samples, formed prior to electrospraying. The data presented above, however, where CID fragments formed in MS/MS parallel those seen in a non-CID experiment, strongly suggest that the electrospray process itself can produce fragmentation of $Au_{25}L_{18}$ nanoparticles. That this can occur has been suggested in other experiments on various analytes.[23−25]

Another instance of Au_4L_4 detection under non-CID conditions is found in the ESI-TOF mass spectrum in Figure 5 of a nanoparticle traditionally referred to as "Au_{140}", though recent literature has assigned it as either $Au_{144}L_{59}$[18] or $Au_{144}L_{60}$.[52] In this experiment, the nanoparticle (and consequently the low mass fragment) had been cationized by exchanging the thiolate

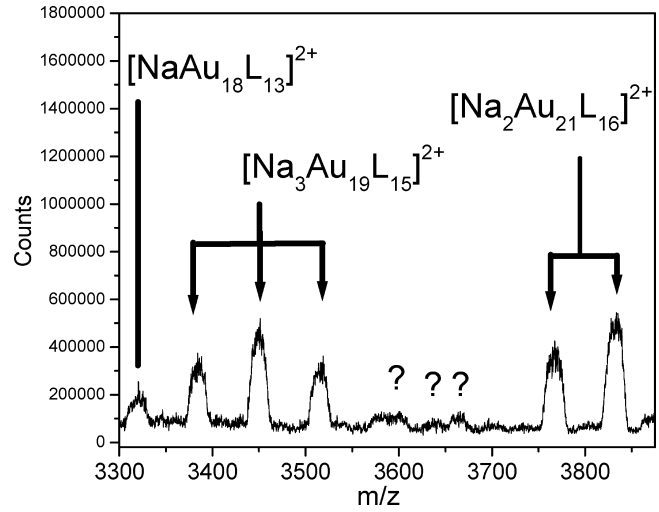

Figure 6. ESI-QQQ-MS/MS spectrum of high *m/z* region fragment ions produced from selected precursor $[Na_4Au_{25}(SC2Ph)_8(SPEG)_{10}]^{3+}$ (m/z = 2929). The mass of these species is obtained by simply multiplying the value of their charge state by the *x*-axis value. Question marks are peaks that could not be assigned with certainty.

$[\text{-}SC_{11}N^+(CH_3)_3][Cl^-]$, or -S-TMA$^+$, onto the parent Au_{144}, which had been prepared with a hexanethiolate shell. No other types of familiar fragments were identified. Theory[52] suggests that $Au_{144}L_{60}$ is composed of a Au_{114} core surrounded by 30 AuL_2 units. The AuL_2 units are not detected in our experiment, which further suggests that Au_4L_4 is the result of rearrangements of the surface units of variously sized nanoparticles.

In attempting to trace the lineage of small nanoparticle fragments such as those shown in Figure 3, one must keep in mind that such fragments either may be primary fragments from the initial precursor $Au_{25}L_{18}$ nanoparticle or may instead have precursorage from large fragments formed from the initial precursor or both. Detection of large fragments is thus a significant step, and indeed MALDI data[22,23] have revealed high-mass fragments from $Au_{25}(SC2Ph)_{18}$ nanoparticles that correspond to losses of multiple AuL units. In the present study, larger fragments were seen in ESI-QQQ-MS/MS mass spectra as shown in Figure 6 from CID of the selected molecular ion $[Na_4Au_{25}(SC2Ph)_8(SPEG)_{10}]^{3+}$ (m/z = 2929). Again we see multiple fragment ion masses, spaced by 130 Da, reflecting the distribution of different numbers of the -SC2Ph and -SPEG ligands on the fragments. Figure 7 shows high mass CID fragments from the selected molecular ion $[Na_5Au_{25}(SC2Ph)_7(SPEG)_{11}]^{4+}$ (m/z = 2235). The presence of fragment ion peaks at *m/z* values *higher* than the precursor molecular ion $[Na_5Au_{25}(SC2Ph)_7(SPEG)_{11}]^{4+}$ provided a useful confirmation of the combined task, here and earlier,[20−22,31] of assigning charge state and composition from such spectra.

Consideration of the spectra in Figures 6 and 7 reveals, however, few plausible *one-step* routes of fragmentation of the precursor ion into the large fragment and into one of the small units in Figure 3. From $[Na_5Au_{25}(SC2Ph)_7(SPEG)_{11}]^{4+}$ in Figure 7, one plausible reaction is

(52) Lopez-Acevedo, O.; Akola, J.; Whetten, R. L.; Gronbeck, H.; Hakkinen, H. *J. Phys. Chem. C* **2009**, *113*, 5035–5038.

$$[Na_5Au_{25}{}^{1-}(SC2Ph)_7(SPEG)_{11}]^{4+} \rightarrow [Na_3Au_{24}{}^{0}L_{16}]^{3+} + [Na_2Au^{1-}L_2]^{1+}$$

where both product ions can be found as intense peaks: $[Na_3Au_{24}L_{16}]^{3+}$ in Figure 7 around 2718 *m/z* and $[Na_2AuL_2]^{1+}$ in Figure 3 around 778 Da. Note that the charge of the parent fragment is conserved in the total charge of the products and that changes occur in the electronic charge of one of the nanoparticle fragments. In a similar example, from $[Na_3Au_{21}{}^{0}L_{16}]^{3+}$ in Figure 7, one reaction could be

$$[Na_3Au_{21}{}^{0}L_{16}]^{3+} \rightarrow [Na_3Au_{18}{}^{0}L_{13}]^{2+} + [Na_2Au_3{}^{0}L_3]^{1+}$$

where $[Na_2Au_{18}{}^{0}L_{13}]^{2+}$ can be found in Figure 7 and $[NaAu_3{}^{0}L_3]^{1+}$ in Figure 3.

On the other hand, the seemingly plausible analogous reaction in which $[Na_3Au_{19}L_{15}]^{2+}$ (Figure 6) loses the same moiety $[Na_2AuL_2]^{1+}$

$$[Na_3Au_{19}{}^{1-}L_{15}]^{2+} \rightarrow [NaAu_{18}{}^{1+}L_{13}]^{2+} + [Na_2Au^{1-}L_2]^{1+} + e^-$$

is not charge balanced and would require an electron loss step. Further consideration of the formation of other large fragments in Figures 6 and 7 directly from the selected precursors $[Na_4Au_{25}(SC2Ph)_8(SPEG)_{10}]^{3+}$ and $[Na_5Au_{25}(SC2Ph)_7(SPEG)_{11}]^{4+}$ shows that none can be formed by a *single* fragmentation step that loses any of the small fragments discussed in Figure 3. Specifically, except for $[Na_3Au_{24}{}^{0}L_{16}]^{3+}$, all of the others require loss of a fragment containing *more Au than ligand*. Thus, forming $[Na_3Au_{19}L_{15}]^{2+}$ in Figure 6 requires loss of $[NaAu_6L_3]^{1+}$ from $[Na_4Au_{25}L_{18}]^{3+}$ and forming $[Na_2Au_{21}L_{16}]^{2+}$ in Figure 6 requires a loss of $[NaAu_4L_2]^{1+}$. Such Au-rich fragments have not been identified. Analogous gaps appear if one considers loss of $[NaAu_2L_2]^{1+}$, $[Na_2Au_2L_3]^{1+}$, $[NaAu_3L_3]^{1+}$, and $[NaAu_4L_4]^{1+}$ from the precursor ion $[Na_5Au_{25}(L)_{18}]^{4+}$. None of the expected large fragment ions in Figures 6 and 7 can be recognized. It would appear that formation of the large nanoparticle fragments in Figures 6 and 7 occurs by losses not recognized by the small fragment species in Figure 3 and/or by (undetectable) loss of neutrals high in Au content. Thus, although both of the CID precursors $[Na_4Au_{25}(SC2Ph)_8(SPEG)_{10}]^{3+}$ and $[Na_5Au_{25}(SC2Ph)_7(SPEG)_{11}]^{4+}$ yield $[Au_{21}L_{16}]^{2+}$ and $[Au_{18}L_{13}]^{2+}$ as fragments (though with differing numbers of Na^+ ions due to difference in number of Na^+ ions of precursor ions), the detailed manner in which this occurs is at this point unclear.

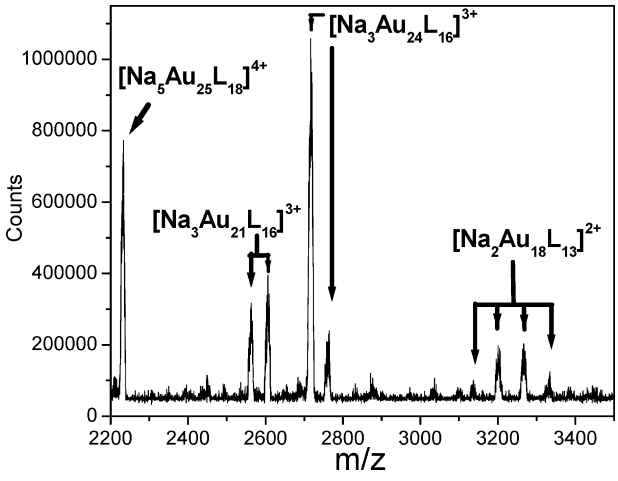

Figure 7. ESI-QQQ-MS/MS of high *m/z* region fragment ions produced from selected precursor $[Na_5Au_{25}(SC2Ph)_7(SPEG)_{11}]^{4+}$ ($m/z = 2235$). The mass of these species is obtained by simply multiplying the value of their charge state by the *x*-axis value. Samples are dissolved in methanol with NaOAc. Presence of peaks at higher *m/z* values than molecular ion confirms multiple charging.

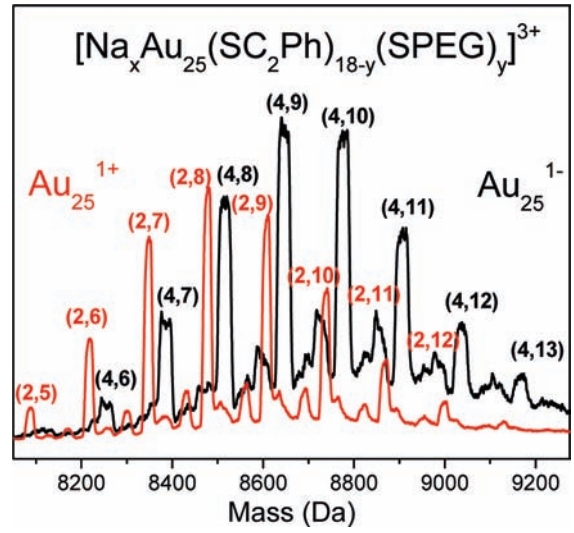

Figure 8. Two ESI-QQQ-MS spectra of PEGylated Au_{25} from the same synthetic batch, where the black curve is the native state of Au_{25} ($Au_{25}{}^{1-}$) and the red curve is oxidized Au_{25} ($Au_{25}{}^{1+}$). The labeling is (*x*,*y*). The red curve has peaks that overlap with some in the black curve, which are minor populations of oxidized nanoparticles in the latter and which were minor unassigned peaks in ref 20. The fragmentation of the oxidized sample produced the same familiar fragments seen for the native state sample.

It is further notable that no fragments with metal contents from Au_5 to Au_{17} (which includes compositions in which the inner Au_{13} core is eroded) were identified at all. This suggests that some formed fragment species are quite unstable, and degrade on time scales too short to be observed.

In mass spectrometry of peptides, it has been reported that the choice of alkali metal ions can substantially change the fragment spectrum.[53] To test for such an effect, KOAc was employed in ESI experiments; the fragmentation pattern was unchanged as shown by the spectral comparison in Figure S-6 (see Supporting Information). Another test concerned the possible effect of the redox state of the $Au_{25}L_{18}$ nanoparticle on the ESI spectra. In a few experiments on PEGylated Au_{25} nanoparticles, the sample was left in solution at room temperature for up to 1 h, which has been suspected to cause oxidation to the $Au_{25}{}^{0}$ and $Au_{25}{}^{1+}$ states, as inferred by the solution becoming cloudy. Suspicion of oxidation was confirmed during data analysis when composition assignments matched to changes in core charges, as shown in Figure 8. The oxidized nanoparticle assignments confirm previous[20] observations of "minor peaks" (e.g., seen at low intensities). The pattern of fragmentation between $Au_{25}{}^{1-}$ and $Au_{25}{}^{1+}$ appears to be identical. This is an interesting result, because theoretical calculations suggest that Au−S bond energies[54] differ with the core charge state.

A complete description and understanding of the route for fragmentation of $Au_{25}L_{18}$ is not realized in this study. There are several possible reasons. For example, the -SPEG based cationization dictates which species are most sensitively detected

(53) Bensadek, D.; Monigatti, F.; Steen, J. A. J.; Steen, H. *Int. J. Mass Spectrom.* **2007**, *268*, 181–189.
(54) Parker, J. F.; Choi, J.-P.; Wang, W.; Murray, R. W. *J. Phys. Chem. C* **2008**, *112*, 13976–13981.

by the instrument. Another possible reason is the low stability of some fragments formed (such as Au-rich ones). Further experiments utilizing ESI-FT-ICR-MS/MS revealed that several of the low mass fragments could be isolated and fragmented to form the other lower mass fragments (data not shown); for example, Au_4L_4 fragmented into Au_3L_3, and isolation and fragmentation of Au_3L_3 resulted in Au_2L_3, all species seen in Figure 3. The fact that the low mass fragments can fragment further may in part explain why there are some minor differences in the low mass fragments formed from the selected precursor ions, 2929 and 2235 *m*/*z*.

Conclusion

CID of $Na_xAu_{25}(SPh)_{18-y}(SPEG)_y$ results in fragmentation of the known semi-rings, which have been very clearly characterized via X-ray crystallography.[31] Some of the fragments detected have been supported in the literature by theory or by experiments under different instrumental conditions. The presence or absence of certain species can be explained by several factors, including stability within the instrument, ionizability, and bond energetics. The formation of some fragments may be favored from stabilities predicted from the "superatom" shell-closing electron count rule ($n^* = N - M - z$, where N is the core metal atom count, M is the number of ligands, and z is the core charge).[55] The most intense high mass fragment peak, for $[Na_3Au_{24}L_{16}]^{3+}$ (Figure 7) does in fact have a closed shell electron count of 8 ($24 - 16 - (-1) = 8$), the same as its precursor, $[Na_5Au_{25}L_{18}]^{4+}$. The other observed heavy fragments, on the other hand, do not.

The ligand shell, being a vehicle for cationization, may affect the fragmentation process. Recent work by the Cliffel group[54] shows that the choice of tiopronin versus glutathione dictated the type of fragment for Au_{102} detected under non-CID conditions. The importance of the ligand shell must, however, not be overstated, as the ligand primarily determines the instrumental ability to detect fragments and various methods have shown that $Au_{25}L_{18}$ dissociates into typically predictable fragments (Au_1L_x-Au_4L_x_ regardless of ligand. In this paper, we've shown that for ESI, a dependable method for detection of $Au_{25}L_{18}$ fragments is PEGylation and coordination to an alkali metal acetate salt. We've also shown that CID results are consistent with other fragmentation methods and that dissociation of the semi-rings is common and the 13 Au atom core tends to be preserved. Only with certain "hard" ionization methods such as FAB[28] is systematic fragmentation of the core (Au_{13}) observed.

Acknowledgment. This research was supported in part by the National Science Foundation. The Molecular Weight Calculator is supported by the National Institutes of Health and the Department of Energy. We are grateful to Gary Glish, University of North Carolina at Chapel Hill, Dept. of Chemistry, and Kellen Harkness from Professor Cliffel's group, Vanderbilt University, Dept. of Chemistry, for helpful discussions, as well as Sohrab Habibi, University of North Carolina at Chapel Hill, Dept. of Chemistry, for access to ESI mass spectral instrumentation. We also thank Hannu Hakkinen and Olga Lopez Acevedo, University of Jyväskylä, Finland, for sharing some results of ongoing, related calculations.

Supporting Information Available: Supplementary mass spectra. This material is available free of charge via the Internet at http://pubs.acs.org.

JA905787Y

(55) Walter, M.; Akola, J.; Lopez-Acevedo, O.; Jadzinsky, P. D.; Calero, G.; Ackerson, C. J.; Whetten, R. L.; Gronbeck, H.; Hakkinen, H. *Proc. Natl. Acad. Sci. U.S.A.* **2008**, *105*, 9157–9162.